Waveguide loss reduction of lateral-current-injection type GaInAsP/InP membrane Fabry–Pérot laser

2017 Jpn. J. Appl. Phys. 56 050311

(http://iopscience.iop.org/1347-4065/56/5/050311)

Japanese Journal of Applied Physics **56**, 050311 (2017)
https://doi.org/10.7567/JJAP.56.050311

RAPID COMMUNICATION

Waveguide loss reduction of lateral-current-injection type GaInAsP/InP membrane Fabry–Pérot laser

Takahiro Tomiyasu[1*], Takuo Hiratani[1], Daisuke Inoue[1], Nagisa Nakamura[1], Tomohiro Amemiya[1,2], Nobuhiko Nishiyama[1,2], and Shigehisa Arai[1,2]

[1]*Department of Electrical and Electronic Engineering, Tokyo Institute of Technology, Meguro, Tokyo 152-8552, Japan*
[2]*Institute of Innovative Research, Tokyo Institute of Technology, Meguro, Tokyo 152-8552, Japan*

*E-mail: tomiyasu.t.aa@m.titech.ac.jp

Received February 13, 2017; accepted March 27, 2017; published online April 20, 2017

We investigated the waveguide loss of lateral-current-injection (LCI) type GaInAsP/InP membrane Fabry–Pérot lasers by adopting low-doped p-InP cap and side cladding layers. An internal quantum efficiency of 75% was obtained, and waveguide loss was reduced to 22 cm^{-1}, which was approximately half of that in our previous report. Further, a differential quantum efficiency higher than 50% was obtained for devices with cavity length less than 400 μm. These results indicate the possibility of sub-mA threshold current and high-efficiency operation of LCI type membrane distributed feedback and distributed-reflector lasers with active region length less than 100 μm.

With the scaling of silicon CMOS technology, the performance of LSIs has improved according to the scaling rule.[1)] Recently, it was predicted that the progress of LSIs will soon confront limitations due to serious problems such as signal delay and Joule heating in the global wiring layers. In order to overcome these problems, the replacement of electrical global wiring with on-chip optical interconnections has been investigated extensively.[2–5)] The light source of on-chip interconnections should have a small footprint, ultralow power consumption, and high-efficiency operation. Several research groups investigated ultralow-power-consumption semiconductor lasers such as vertical-cavity surface-emitting lasers (VCSEL),[6,7)] microdisk lasers,[8,9)] and photonic crystal lasers.[10–12)] The available energy of the semiconductor laser was estimated to be less than 100 fJ/bit,[4)] which implies that power consumption should be less than 1 mW at 10 Gbps operation in the on-chip optical interconnection system. In addition, we estimated that the light output should be greater than 0.16 mW at 10 Gbps operation under the assumption of a link budget of 5 dB.[13)]

In order to realize such optical interconnects, we have proposed semiconductor membrane lasers for low power consumption and high-efficiency operation,[14)] and we demonstrated the low-threshold operation of a lateral-current-injection (LCI) type membrane distributed feedback (DFB) laser under room-temperature continuous-wave optical pumping.[15)] The membrane structure, which consists of a thin (150–250 nm) semiconductor core layer sandwiched between low-refractive-index dielectric cladding layers, provides strong optical confinement in the semiconductor core layer and enables the development of small-footprint devices.[16)] This strong optical confinement leads to enhanced modal gain and low-threshold-current operation compared with conventional lasers.[17)] Moreover, this structure has a large index-coupling coefficient of the grating, and we achieved a low-threshold-current DFB laser with a short cavity length of 50 μm.[18)] For high-efficiency operation, we adopted a distributed-reflector (DR) structure that consists of a DFB region with a distributed Bragg reflector at its rear side. Even membrane DR lasers with low-threshold and high-efficiency operation as well as asymmetric light output have been demonstrated,[19)] but the light output power was insufficient to realize the desired system of optical interconnects owing to a high waveguide loss of 42 cm^{-1}.[20)]

In this study, we investigated the waveguide loss of membrane Fabry–Pérot (FP) lasers consisting of p-type InP layers with different doping concentrations. From the cavity length dependence of those devices, we evaluated the p-InP doping-concentration dependence of not only the waveguide loss but also the internal quantum efficiency.

Figure 1(a) shows schematic cross sections of an LCI-FP laser with a core thickness of 400 nm on a semi-insulating (SI) InP substrate[21)] (on the left), a membrane FP laser with a core thickness of 220 nm including a p-InP cap layer ($N_{A,cap} = 4 \times 10^{18}$ cm^{-3}) bonded on a Si substrate[20)] (on the center), and a membrane FP laser with a core thickness of 270 nm including a p-InP cap layer ($N_{A,cap} = 3 \times 10^{17}$ cm^{-3}) bonded on a Si substrate (on the right). Since surface recombination speed of GaInAsP optical confinement layer (OCL, indicated by yellow) is much larger than that of InP and the hole mobility is much lower than that of the electron mobility in InP, p-InP cap layer was grown on the top GaInAsP OCL so as to suppress the surface recombination and improve an internal quantum efficiency. Figure 1(b) shows mode profiles corresponding to these lasers based on the fabricated devices. In the case of the LCI laser on the SI-InP substrate, the mode field is pulled to the SI-InP substrate owing to the low refractive-index difference between the core layer and SI-InP substrate. On the other hand, the mode field of the membrane lasers spreads along the horizontal direction and is strongly confined to the active layer because of the high-index-contrast structure. Table I lists material absorption coefficients for the estimation of waveguide losses of these lasers. The doping concentrations of the p-InP and n-InP side cladding layers were derived from secondary ion mass spectrometry measurement. In this work, the absorption coefficients of $Ga_{0.22}In_{0.78}As_{0.81}P_{0.19}$ (well), p-InP ($N_A = 2 \times 10^{18}$ cm^{-3}), p-InP ($N_A = 5 \times 10^{17}$ cm^{-3}), p-InP ($N_A = 3 \times 10^{17}$ cm^{-3}), and n-InP ($N_D = 2 \times 10^{18}$ cm^{-3}) were calculated to be 100, 40, 10, 6, and 2 cm^{-1}, respectively.

Figure 2 shows the estimated waveguide losses of these lasers and compositions. The waveguide losses were calculated by integrating the product of material loss and optical mode profile. In the case of the LCI laser on the SI-InP substrate, the waveguide loss was estimated to be 5.0 cm^{-1}, while an experimental value of 5.1 cm^{-1} had been reported.[21)] On the other hand, the waveguide loss of the membrane laser with a high-doped p-InP cap layer ($N_{A,cap} = 4 \times 10^{18}$ cm^{-3})

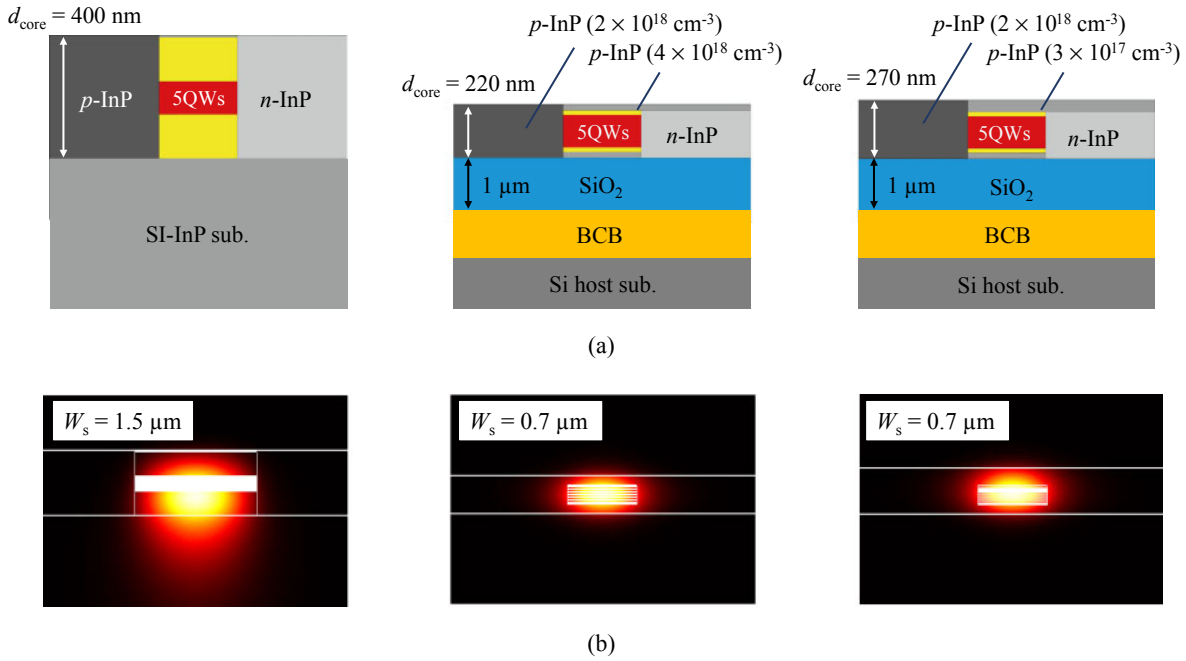

Fig. 1. (Color online) (a) Schematic cross sections and (b) mode field profiles of LCI laser on SI-InP substrate (left) and LCI membrane lasers (center and right). Five quantum-wells (5QWs) are sandwiched by GaInAsP optical confinement layers (OCLs).

Table I. Material absorption coefficients for estimation of waveguide loss.

Material	Absorption coefficient (cm^{-1})
$Ga_{0.22}In_{0.78}As_{0.81}P_{0.19}$ (well)	100
p-InP (2×10^{18} cm^{-3})	40
p-InP (5×10^{17} cm^{-3})	10
p-InP (3×10^{17} cm^{-3})	6
n-InP	2

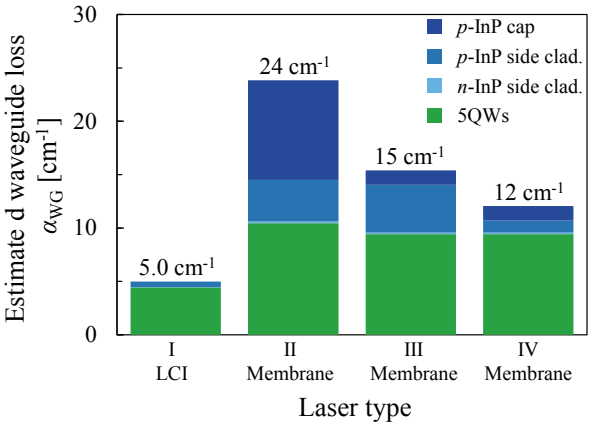

Fig. 2. (Color online) Estimated waveguide loss with respect to composition. Laser types I to IV indicate the LCI laser,[21] membrane laser in the previous work,[20] membrane laser with a low-doped p-InP cap layer, and membrane laser with low-doped p-InP cap and side cladding layers.

was estimated to be 24 cm^{-1} because of the higher mode field in the p-InP cap and side cladding layers, while an experimental waveguide loss of 42 cm^{-1} was reported.[20] This large difference between the theoretical and experimental values is probably attributed to the scattering loss caused by the roughness arising from the photolithography process of the mesa stripe and regrowth process by organometallic vapor phase epitaxy (OMVPE). Because the electric field is strongly confined into the thin semiconductor core layer, the roughness causes a large scattering loss. The waveguide loss of the membrane lasers was estimated to be much higher than that of the LCI laser on the SI-InP substrate because of the higher optical absorption not only in the active layer due to strong optical confinement, but also in the p-InP cap and side cladding layers due to strong leak from the active layer, as shown in Fig. 1(b). Thus, the adoption of a low-doped p-InP cap layer is effective for waveguide loss reduction without the increase of differential resistance because the injection current does not flow in the p-InP cap layer. The waveguide loss could be reduced to 15 cm^{-1} by adopting a p-InP cap layer with low concentration ($N_{A,cap} = 3 \times 10^{17}$ cm^{-3}). Moreover, it could be reduced to 12 cm^{-1} by adopting a low-doped p-InP cap layer ($N_{A,cap} = 3 \times 10^{17}$ cm^{-3}) and p-InP side cladding layer ($N_{A,cap} = 5 \times 10^{17}$ cm^{-3}), while the increase of differential resistance was anticipated.

Next, we fabricated membrane FP lasers with a low-doped p-InP cap layer ($N_{A,cap} = 3 \times 10^{17}$ cm^{-3}) and a stripe width of 0.7 μm, as shown in Fig. 1(a) (on the right). The fabrication process was almost same as that of our previous work.[20] We also fabricated membrane FP lasers with a low-doped p-InP cap layer ($N_{A,cap} = 3 \times 10^{17}$ cm^{-3}) and side cladding layer ($N_{A,cap} = 5 \times 10^{17}$ cm^{-3}) and stripe width of 0.6 μm. Figure 3 shows the current–light output (*I*–*L*) and current–voltage (*I*–*V*) characteristics of the fabricated membrane FP lasers. The cavity length of devices with low-doped p-InP cap and side cladding layers was 830 μm, and that of devices with only a low-doped p-InP cap layer was 900 μm. In order to clarify the effect of doping concentration of the p-InP side cladding layer, devices with longer cavity length were chosen for comparison. In the case of the device with a low-doped p-InP cap layer alone, a threshold current I_{th} of 5.6 mA (corresponding threshold current density J_{th} of 890 A/cm^2),

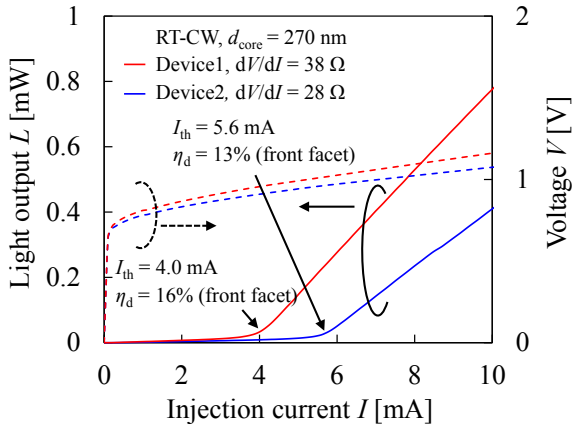

Fig. 3. (Color online) Light output and voltage–current characteristics of membrane FP lasers. Device 1 denotes the device with low-doped p-InP cap and side cladding layers, a stripe width W_s of 0.6 μm, and a cavity length L of 830 μm. Device 2 denotes the one with a low-doped p-InP cap layer, W_s of 0.7 μm, and L of 900 μm.

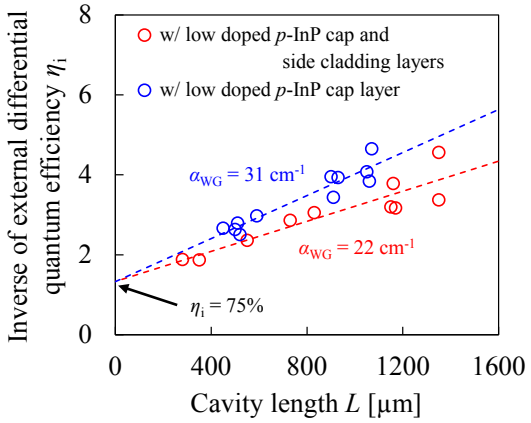

Fig. 4. (Color online) Measured cavity length dependence of the inverse of the differential quantum efficiency η_d.

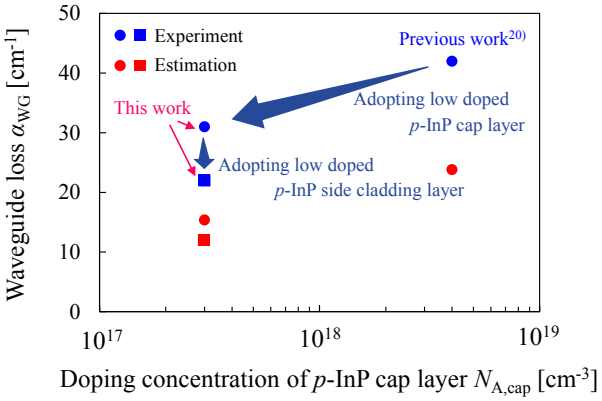

Fig. 5. (Color online) Dependence of waveguide loss on the doping concentration of p-InP cap layer.

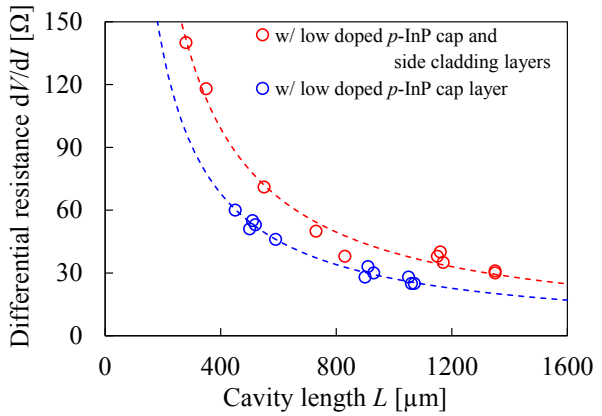

Fig. 6. (Color online) Measured and fitting curve of cavity length dependence of the differential resistance.

an external differential quantum efficiency from the front facet η_d of 13%, and a differential resistance dV/dI of 28 Ω were obtained. On the other hand, in the case of the device with low-doped p-InP cap and side cladding layers, an I_{th} of 4.0 mA (J_{th} of 800 A/cm^2), an η_d of 13%, and a dV/dI of 38 Ω were obtained. Owing to the reduction of doping concentration of the p-InP side cladding layer, improvements in both threshold current and external differential quantum efficiency were obtained, while the differential resistance was increased.

Figure 4 shows the measured cavity length dependence of the inverse of the differential quantum efficiency η_d. Assuming the facet reflectivities of both facets are equal, the relation between cavity length and η_d is expressed as

$$\frac{1}{\eta_d} = \frac{1}{\eta_i}\left[1 + \frac{\alpha_{WG}L}{\ln(1/R)}\right], \quad (1)$$

where η_i is the internal quantum efficiency, R is the facet reflectivity, L is the cavity length, and α_{WG} is the waveguide loss. From linear extrapolation using Eq. (1), we obtained an internal quantum efficiency η_i of 75% and waveguide loss α_{WG} of 31 cm^{-1} in the case of membrane FP lasers with a low-doped p-InP cap layer alone. Further, an internal quantum efficiency η_i of 75% and a waveguide loss α_{WG} of 22 cm^{-1} were obtained in the case of membrane FP lasers with low-doped p-InP cap and side cladding layers. The η_i of 75% is the same as that in our previous work on membrane FP lasers.[20] These high internal quantum efficiencies indicate that the fabrication process, especially the two-step OMVPE regrowth, has been firmly established.

As can be seen in Fig. 4, the differential quantum efficiency higher than 50%, which seems to be a good value for lasers emitting at 1.5–1.6 μm, was obtained with a cavity length of 300–350 μm.

Figure 5 shows the dependence of waveguide loss on the doping concentration of the p-InP cap layer. The waveguide loss was reduced from 42 to 31 cm^{-1} by adopting a p-InP cap layer with lower concentration, and it was further reduced to 22 cm^{-1} by adopting both p-InP cap and side cladding layers of low concentration. However, the waveguide loss α_{WG} of 22 cm^{-1} is still larger than the estimated waveguide loss of 12 cm^{-1} as well as that in the previous work.[20] As mentioned above, this is probably attributed to the scattering loss strongly influenced by the roughness around the mesa stripe.

Figure 6 shows the measured (indicated by open circles) cavity length dependence of the differential resistance, where dashed lines represent least-squares fitting curves of experimental results. Assuming the contribution of the resistance of the p-InP side cladding layer $R_{p\text{-}InP}$ is dominant in the differential resistance because it is much higher than the resistance of the n-InP side cladding layer, the resistance of the p-InP side cladding layer was derived using the following equation:

$$R_{\text{p-InP}} = \rho_{\text{p-InP}} \frac{W}{d_{\text{core}} L}, \quad (2)$$

where $\rho_{\text{p-InP}}$ is the resistance of the p-InP side cladding layer, W is the distance from the p-side electrode to the active region, d_{core} is the thickness of the core layer, and L is the cavity length. By using Eq. (2) and the measured distance from the p-side electrode to the active region W of 3 μm, the resistance of the p-InP side cladding region was obtained as 0.34 Ω·cm for devices with low-doped p-InP cap and side cladding layers, while it was obtained as 0.23 Ω·cm for those with only the low-doped p-InP cap layer. Although the differential resistance of the former devices was approximately 1.5 times that of the latter ones, it can be reduced by shortening the distance W between the p-side electrode and active region. Thus, the design of membrane DFB and DR lasers for high-efficiency operation requires not only low-doped p-InP cap and side cladding layers, but also a short distance W between the p-side electrode and active region.

In conclusion, we demonstrated the waveguide loss reduction of membrane FP lasers by reducing the concentration of p-InP cap and side cladding layers. A waveguide loss of 31 cm^{-1} and an internal quantum efficiency of 75% were obtained for devices with a low-doped p-InP cap layer alone. Further, a waveguide loss of 22 cm^{-1} and an internal quantum efficiency of 75% were obtained for devices with low-doped p-InP cap and side cladding layers. These results indicate that the fabrication process, especially the two-step OMVPE regrowth, is firmly established and that the moderately high-efficiency operation of membrane DFB and DR lasers can be obtained by shortening the distance from the p-side electrode to the active region, while differential resistances increased on reducing the concentration of the p-InP side cladding layer.

Acknowledgments The authors would like to thank Professors M. Asada, Y. Miyamoto, T. Mizumoto, and S. Akiba of the Tokyo Institute of Technology, Tokyo, Japan, for fruitful discussions and comments. This work was supported by JSPS KAKENHI Grant Numbers 15H05763, 25709026, 15J04654, 15J11776, and 16H06082 and JST-CREST.

1) R. H. Dennard, F. H. Gaensslen, V. L. Rideout, E. Bassous, and A. R. LeBlanc, IEEE J. Solid-State Circuits **9**, 256 (1974).
2) M. Haurylau, G. Chen, H. Chen, J. Zhang, N. A. Nelson, D. H. Albonesi, E. G. Friedman, and P. M. Fauchet, IEEE J. Sel. Top. Quantum Electron. **12**, 1699 (2006).
3) G. Chen, H. Chen, M. Haurylau, N. A. Nelson, D. H. Albonesi, P. M. Fauchet, and E. G. Friedman, Integration—VLSI J. **40**, 434 (2007).
4) D. A. B. Miller, Proc. IEEE **97**, 1166 (2009).
5) K. Ohashi, K. Nishi, T. Shimizu, M. Nakada, J. Fujikata, J. Ushida, S. Torii, K. Nose, M. Mizuno, H. Yukawa, M. Kinoshita, N. Suzuki, A. Gomyo, T. Ishi, D. Okamoto, K. Furue, T. Ueno, T. Tsuchizawa, T. Watanabe, K. Yamada, S. Itabashi, and J. Akedo, Proc. IEEE **97**, 1186 (2009).
6) P. Moser, W. Hofmann, P. Wolf, J. A. Lott, G. Larisch, A. Payusov, N. N. Ledentsov, and D. Bimberg, Appl. Phys. Lett. **98**, 231106 (2011).
7) A. Kasukawa, IEEE Photonics J. **4**, 642 (2012).
8) M. Fujita, R. Ushigome, and T. Baba, Electron. Lett. **36**, 790 (2000).
9) J. Van Campenhout, P. Rojo-Romeo, P. Regreny, C. Seassal, D. Van Thourhout, S. Verstuyft, L. Di Cioccio, J.-M. Fedeli, C. Lagahe, and R. Baets, Opt. Express **15**, 6744 (2007).
10) S. Matsuo, A. Shinya, T. Kakitsuka, K. Nozaki, T. Segawa, T. Sato, Y. Kawaguchi, and M. Notomi, Nat. Photonics **4**, 648 (2010).
11) B. Ellis, M. A. Mayer, G. Shambat, T. Sarmiento, J. Harris, E. E. Haller, and J. Vučković, Nat. Photonics **5**, 297 (2011).
12) S. Matsuo, T. Sato, K. Takeda, A. Shinya, K. Nozaki, H. Taniyama, M. Notomi, K. Hasebe, and T. Kakitsuka, IEEE J. Sel. Top. Quantum Electron. **19**, 4900311 (2013).
13) T. Hiratani, T. Shindo, K. Doi, Y. Atsuji, D. Inoue, T. Amemiya, N. Nishiyama, and S. Arai, IEEE J. Sel. Top. Quantum Electron. **21**, 299 (2015).
14) S. Arai, N. Nishiyama, T. Maruyama, and T. Okumura, IEEE J. Sel. Top. Quantum Electron. **17**, 1381 (2011).
15) T. Okamoto, N. Nunoya, Y. Onodera, T. Yamazaki, S. Tamura, and S. Arai, IEEE J. Sel. Top. Quantum Electron. **9**, 1361 (2003).
16) T. Okumura, T. Koguchi, H. Ito, N. Nishiyama, and S. Arai, Appl. Phys. Express **4**, 042101 (2011).
17) S. Sakamoto, H. Naitoh, M. Ohtake, Y. Nishimoto, S. Tamura, T. Maruyama, N. Nishiyama, and S. Arai, IEEE J. Sel. Top. Quantum Electron. **13**, 1135 (2007).
18) D. Inoue, J. Lee, T. Hiratani, Y. Atsuji, T. Amemiya, N. Nishiyama, and S. Arai, Opt. Express **23**, 7771 (2015).
19) T. Hiratani, D. Inoue, T. Tomiyasu, Y. Atsuji, K. Fukuda, T. Amemiya, N. Nishiyama, and S. Arai, Appl. Phys. Express **8**, 112701 (2015).
20) D. Inoue, J. Lee, K. Doi, T. Hiratani, Y. Atsuji, T. Amemiya, N. Nishiyama, and S. Arai, Appl. Phys. Express **7**, 072701 (2014).
21) M. Futami, T. Shindo, T. Koguchi, K. Shinno, T. Amemiya, N. Nishiyama, and S. Arai, IEEE Photonics Technol. Lett. **24**, 888 (2012).